DOI: 10.1021/ic100301q

Inorganic Chemistry
Article

Cyanide-Bridged Fe(III)−Mn(III) Bimetallic Systems Assembled from the *fac*-Fe Tricyanide and Mn Schiff bases: Structures, Magnetic Properties, and Density Functional Theory Calculations

Hyun Young Kwak,[†] Dae Won Ryu,[†] Jin Wuk Lee,[†] Jung Hee Yoon,[†] Hyoung Chan Kim,[‡] Eui Kwan Koh,[§] Jamin Krinsky,[∥] and Chang Seop Hong*[,†]

[†]*Department of Chemistry (BK21), Korea University, Seoul 136-713, Korea,* [‡]*National Fusion Research Institute, Daejeon 305-333, Korea,* [§]*Nano-Bio System Research Team, Korea Basic Science Institute, Seoul 136-713, Korea, and* [∥]*Department of Chemistry, University of California, Berkeley, California 94720-1460*

Received February 12, 2010

Reaction of $[(Tp)Fe(CN)_3]^-$ [Tp = hydrotris(pyrazolyl)borate] with respective Mn(III) Schiff bases led to the formation of four dimeric molecules, $[(Tp)Fe(CN)_3][Mn(1\text{-napen})(H_2O)]\cdot MeCN\cdot 4H_2O$ [**1**; 1-napen = *N*,*N*′-ethylenebis(2-hydroxy-1-naphthylideneiminato) dianion], $[(Tp)Fe(CN)_3][Mn(5\text{-Clsalen})(H_2O)]$ [**2**; 5-Clsalcy = *N*,*N*′-(trans-1,2-cyclohexanediyl-ethylene)bis(5-chlorosalicylideneiminato) dianion], $[(Tp)Fe(CN)_3][Mn(2\text{-acnapen})(MeOH)]\cdot MeOH$ [**3**; 2-acnapen = *N*,*N*′-ethylenebis(1-hydroxy-2-acetonaphthylideneiminato) dianion], $[(Tp)Fe(CN)_3][Mn(3\text{-MeOsalen})(H_2O)]$ [**4**; 3-MeOsalen = *N*,*N*′-ethylenebis(3-methoxysalicylideneiminato) dianion], and a one-dimensional (1D) zigzag chain $[(Tp)Fe(CN)_3][Mn(2\text{-acnapen})]\cdot H_2O$ (**5**). The dimers contain multiple intermolecular interactions such as hydrogen bonds, face-to-face $\pi-\pi$ contacts, and edge-to-face CH$-\pi$ forces, raising molecular dimensions from one-dimensional (1D) up to three-dimensional (3D) arrays, whereas there are no $\pi-\pi$ stacking interactions in the 1D chain compound. Magnetic measurements reveal that ferromagnetic couplings are obviously operative between Mn(III) and Fe(III) spin centers transmitted by CN bridges for **1**−**3** and **5**, and antiferromagnetic interactions are however unexpectedly present in **4**. On the basis of the proper spin Hamiltonians, magnetic exchange couplings are estimated to be in the span from 1.79 to 7.48 cm^{-1} for the ferromagnetically coupled systems and −1.40 cm^{-1} for the antiferromagnetic dimer. A slow magnetic relaxation is tangible in **5**, which is in connection with isolated chains devoid of any intermolecular noncovalent interactions. Density Functional Theory (DFT) calculations and comparison of structural parameters suggest that the observed magnetic behaviors are mainly associated with the bending of the Mn−N≡C angle in the bridging pathway.

Introduction

Molecule-based magnetic materials with intriguing properties such as high T_C,[1] dual functions,[2] and photomagnetic characters[3] have been one of hot issues because of their potential applications in magnetic devices. Hexacyanometalates $[A(CN)_6]^{p-}$ (A = V, Cr, Mn, Fe), heptacyanometalates $[B(CN)_7]^{q-}$ (B = Mo, Re), and octacyanometalates $[C(CN)_8]^{r-}$ (C = Mo, W, Nb) have been frequently utilized to fabricate exotic clusters and multidimensional coordination networks.[1,3,4]

Incorporation of anisotropic magnetic characters into discrete or one-dimensional (1D) structural motifs generated slow magnetic relaxations applicable for high-density information storage. The molecular design for single-molecule

*To whom correspondence should be addressed. E-mail: cshong@korea.ac.kr.

(1) Holmes, S. M.; Girolami, G. S. *J. Am. Chem. Soc.* **1999**, *121*, 5593.
(2) (a) Coronado, E.; Galan-Mascaros, J. R.; Gomez-Garcia, C. J.; Laukhin, V. *Nature* **2000**, *408*, 447. (b) Spaldin, N. A.; Fiebig, M. *Science* **2005**, *309*, 391. (c) Sott, J. F. *Science* **2006**, *315*, 954. (d) Eerenstein, W.; Mathur, N. D.; Scott, J. F. *Nature* **2006**, *442*, 759. (e) Andres, R.; Brissard, M.; Gruselle, M.; Train, C.; Vaissermann, J.; Malezieux, B.; Jamet, J.-P.; Verdaguer, M. *Inorg. Chem.* **2001**, *40*, 4633.
(3) (a) Dei, A. *Angew. Chem., Int. Ed.* **2005**, *44*, 1160. (b) Arimoto, Y.; Ohkoshi, S.-i.; Zhong, Z. J.; Seino, H.; Mizobe, Y.; Hashimoto, K. *J. Am. Chem. Soc.* **2003**, *125*, 9240. (c) Herrera, J. M.; Marvaud, V.; Verdaguer, M.; Marrot, J.; Kalisz, M.; Mathonière, C. *Angew. Chem., Int. Ed.* **2004**, *43*, 5468. (d) Ohkoshi, S.-i.; Tokoro, H.; Hozumi, T.; Z, Y.; Hashimoto, K.; Mathonière, C.; Bord, I.; Rombaut, G.; Verlelst, M.; Moulin, C. C. d.; Villain, F. *J. Am. Chem. Soc.* **2006**, *128*, 270. (e) Ohkoshi, S.-i.; Ikeda, S.; Hozumi, T.; Kashiwagi, T.; Hashimoto, K. *J. Am. Chem. Soc.* **2006**, *128*, 5320.
(4) (a) Bennett, M. V.; Long, J. R. *J. Am. Chem. Soc.* **2003**, *125*, 2394. (b) Pradhan, R.; Desplanches, C.; Guionneau, P.; Sutter, J.-P. *Inorg. Chem.* **2003**, *42*, 6607. (c) Withers, J. R.; Li, D.; Jeremy, T.; Ruschman, C.; Parkin, S.; Wang, G.; Yee, G. T.; Holmes, S. M. *Polyhedron* **2007**, *26*, 2353. (d) Kashiwagi, T.; Ohkoshi, S.-i.; Seino, H.; Mizobe, Y.; Hashimoto, K. *J. Am. Chem. Soc.* **2004**, *126*, 5024. (e) Li, D.-f.; Gao, S.; Zheng, L.-m.; Tang, W.-x. *J. Chem. Soc., Dalton Trans.* **2002**, 2805. (f) Podgajny, R.; Balanda, M.; Sikora, M.; Borowiec, M.; Spalek, L.; Kapusta, C.; Sieklucka, B. *Dalton Trans.* **2006**, 2801. (g) Shores, M. P.; Sokol, J. J.; Long, J. R. *J. Am. Chem. Soc.* **2002**, *124*, 2279. (h) Ruiz, E.; Rodríguez-Fortea, A.; Alvarez, S.; Verdaguer, M. *Chem.—Eur. J.* **2005**, *11*, 2135. (i) Visinescu, D.; Desplanches, C.; Imaz, I.; Bahers, V.; Pradhan, R.; Villamena, F. A.; Guionneau, P.; Sutter, J.-P. *J. Am .Chem. Soc.* **2006**, *128*, 10202. (j) Kosaka, W.; Imoto, K.; Tsunobuchi, Y.; Ohkoshi, S.-i. *Inorg. Chem.* **2009**, *48*, 4604. (k) Lim, J. H.; Yoon, J. H.; Kim, H. C.; Hong, C. S. *Angew. Chem., Int. Ed.* **2006**, *45*, 7424.

Published on Web 04/19/2010

magnets (SMMs) and single-chain magnets (SCMs) exhibiting such relaxed magnetizations requires blocked building units capable of restricting structural expansion from high dimensions and magnetically anisotropic sources.[5] Fe(III) bearing precursors $[LFe(CN)_3]^-$, which are *meridionally* or *facially* capped with tridentate N-donor ligands, have been successfully employed in the formation of magnetically coupled systems. For instance, *mer*-$[LFe^{III}(CN)_3]^-$ precursors with chelating ligands of bis(2-pyridylcarbonyl)amidate anion (bpca),[6] 8-(pyridine-2-carboxamido)quinoline anion (pcq),[7] 8-(pyrazine-2-carboxamido)quinoline anion (pzcq),[8] 8-(5-methylpyrazine-2-carboxamido)quinoline anion (mpzcq),[9] and 8-(2-quinolinecarboxamido)quinoline anion (qcq)[10] were prepared. Self-assembly of these molecular units with judicious choices of paramagnetic counterparts produced low-dimensional magnetic families. Moreover, *facial* Fe^{III} tricyanides were designed and they accommodate blocking groups of hydrotris(pyrazolyl)borate (Tp), hydrotris-(3,5-dimethylpyrazol-1-yl)borate (Tp*), tetra(pyrazol-1-yl)-borate (pzTp), and 1,3,5-triaminocyclohexane (tach).[11] The building precursors were often taken to create numerous magnetic systems with molecular and 1D chain structures.[11]

In addition, Mn(III) quadridentate Schiff bases with intrinsic Jahn−Teller elongations in axial directions showed sizable anisotropic characteristics. The Mn Schiff bases maintain two accessible sites for incoming N- or O-donors in a *trans* position. Thus, it would be reasonable to combine the blocked molecular precursors and the Mn Schiff bases in pursuit of low-dimensional anisotropic molecular materials.[12]

A limited number of cyanide-bridged Fe(III)−Mn(III) bimetallic assemblies were structurally and magnetically characterized.[8−10,13] Notably, antiferromagnetic interactions are exclusively visible in *mer*-Fe tricyanide-bridged complexes so far,[8−10] while magnetic properties of *fac*-Fe tricyanide-linked compounds are mostly ferromagnetic with a rare exceptional example.[13] To understand a fundamental magnetic exchange mechanism in cyanide-bridged Fe(III)−Mn(III) systems resorting to the $[(Tp)Fe(CN)_3]^-$ anion, a series of magnetic systems need to be devised. Particularly, dinuclear structures would be beneficial to establish the relationship between structure and magnetic character because they can be analyzed with only one *J* parameter.[14] In this vein we attempted to develop *fac*-(Tp)-$Fe(CN)_3$-based dinuclear Fe(III)−Mn(III) analogues with subtle structural variations.

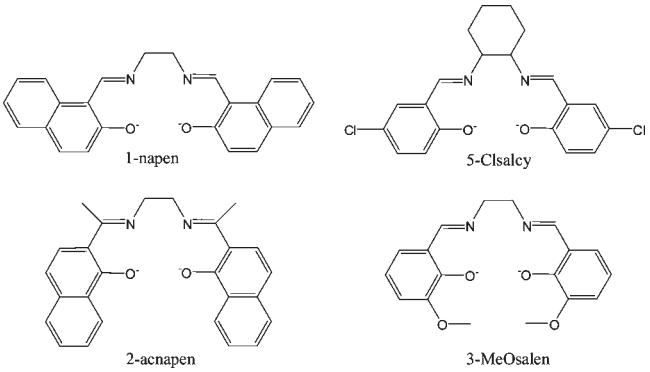

Herein we report the syntheses, structures, and magnetic properties of four dimeric molecules, $[(Tp)Fe(CN)_3][Mn(1\text{-napen})(H_2O)]\cdot MeCN\cdot 4H_2O$ (**1**), $[(Tp)Fe(CN)_3][Mn(5\text{-Clsalen})(H_2O)]$ (**2**), $[(Tp)Fe(CN)_3][Mn(2\text{-acnapen})(MeOH)]\cdot MeOH$ (**3**), and $[(Tp)Fe(CN)_3][Mn(3\text{-MeOsalen})(H_2O)]$ (**4**), which possess many intermolecular forces, as well as a 1D chain compound $[(Tp)Fe(CN)_3][Mn(2\text{-acnapen})]\cdot H_2O$ (**5**). Density functional theory (DFT) calculations and structural considerations support that magnetic natures can be varied relying on the bending of the Mn−N≡C angle in the bridging route. A slow magnetic relaxation is discernible in **5**, which arises from the absence of interchain noncovalent contacts.

Experimental Section

Reagent. $(Ph_4P)[(Tp)Fe(CN)_3]\cdot H_2O$ and Mn Schiff bases were synthesized according to the literature procedures.[12,13b,15] All chemicals and solvents in the synthesis were of reagent grade and used as received. All manipulations were performed under aerobic conditions.

Synthesis. ***Caution!*** *Perchlorate salts of metal compounds with organic ligands are potentially explosive and cyanides are toxic. These materials should be handled with great caution.*

$[(Tp)Fe(CN)_3][Mn(1\text{-napen})(H_2O)]\cdot MeCN\cdot 4H_2O$ (1). A solution of $[Mn(1\text{-napen})(H_2O)]Cl$ (0.10 mmol) in H_2O/MeCN (10 mL) was added to a solution of $(Ph_4P)[(Tp)Fe(CN)_3]\cdot H_2O$ (0.10 mmol) in MeOH/MeCN (1:1 v/v, 10 mL). The brown solution was stirred for 3 min, filtered, slowly evaporated in the dark, which gave brown crystals in 60% yield. Anal. Calcd for $C_{38}H_{39}BFeMnN_{12}O_7$: C, 50.86; H, 4.38; N, 18.73. Found: C, 50.75; H, 3.96; N, 18.54.

$[(Tp)Fe(CN)_3][Mn(5\text{-Clsalen})(H_2O)]$ (2). Addition of $[Mn(5\text{-Clsalen})(H_2O)]ClO_4$ (0.10 mmol) in H_2O/MeCN (1:2 v/v, 10 mL) to a solution of $(Ph_4P)[(Tp)Fe(CN)_3]\cdot H_2O$ (0.10 mmol) in MeOH (10 mL) afforded a brown solution. The solution was stirred for 3 min. The filtered clear solution was left undisturbed

(5) (a) Gatteschi, S.; Sessoli, R. *Angew. Chem., Int. Ed.* **2003**, *42*, 268. (b) Lescouëzec, R.; Toma, L. M.; Vaissermann, J.; Verdaguer, M.; Delgado, F. S.; Ruiz-Pérez, C.; Lloret, F.; Julve, M. *Coord. Chem. Rev.* **2005**, *249*, 2691. (c) Coulon, C.; Miyasaka, H.; Clérac, R. *Struct. Bonding* (*Berlin*) **2006**, *122*, 163.
(6) Lescouëzec, R.; Vaissermann, J.; Toma, M.; Carrasco, R.; Lloret, F.; Julve, M. *Inorg. Chem.* **2004**, *43*, 2234.
(7) Ni, Z.-H.; Kou, H.-Z.; Zhang, L.-F.; Ni, W.-W.; Jiang, Y.-B.; Cui, A.-L.; Ribas, J.; Sato, O. *Inorg. Chem.* **2005**, *44*, 9631.
(8) Kim, J. I.; Yoo, H. S.; Koh, E. K.; Kim, H. C.; Hong, C. S. *Inorg. Chem.* **2007**, *46*, 8481.
(9) Kim, J. I.; Yoo, H. S.; Koh, E. K.; Hong, C. S. *Inorg. Chem.* **2007**, *46*, 10461.
(10) Kim, J. I.; Kwak, H. Y.; Yoon, J. H.; Ryu, D. W.; Yoo, I. Y.; Yang, N.; Koh, E. K.; Park, J.-G.; Lee, H.; Hong, C. S. *Inorg. Chem.* **2009**, *48*, 2956.
(11) (a) Liu, W.; Wang, C.-F.; Li, Y.-Z.; Zuo, J.-L.; You, X.-Z. *Inorg. Chem.* **2006**, *45*, 10058. (b) Wen, H.-R.; Wang, C.-F.; Song, Y.; Gao, S.; Zuo, J.-L.; You, X.-Z. *Inorg. Chem.* **2006**, *45*, 8942. (c) Gu, Z.-G.; Yang, Q.-F.; Liu, W.; Song, Y.; Li, T.-Z.; Zuo, J.-L.; You, X.-Z. *Inorg. Chem.* **2006**, *45*, 8895. (d) Wang, S.; Zuo, J.-L.; Zhou, H.-C.; Choi, H. J.; Ke, Y.; Long, J. R.; You, X.-Z. *Angew. Chem., Int. Ed.* **2004**, *43*, 5940. (e) Li, D.; Parkin, S.; Wang, G.; Yee, G. T.; Prosvirin, A. V.; Holmes, S. M. *Inorg. Chem.* **2005**, *44*, 4903. (f) Li, D.; Parkin, S.; Wang, G.; Yee, G. T.; Clérac, R.; Wernsdorfer, W.; Holmes, S. M. *J. Am. Chem. Soc.* **2006**, *128*, 4214. (g) Yang, J. Y.; Shores, M. P.; Sokol, J. J.; Long, J. R. *Inorg. Chem.* **2003**, *42*, 1403. (h) Wang, S.; Zuo, J.-L.; Gao, S.; Song, Y.; Zhuo, H.-C.; Zhang, Y.-Z.; You, X.-Z. *J. Am. Chem. Soc.* **2004**, *126*, 8900. (i) Zhang, Y.-J.; Liu, T.; Kanegawa, S.; Sato, O. *J. Am. Chem. Soc.* **2010**, *132*, 912. (j) Li, X.-M.; Wang, C.-F.; Ji, Y.; Kang, L.-C.; Zhou, X.-H.; Zuo, J.-L.; You, X.-Z. *Inorg. Chem.* **2009**, *48*, 9166.
(12) Yoon, J. H.; Ryu, D. W.; Kim, H. C.; Yoon, S. W.; Suh, B. J.; Hong, C. S. *Chem.—Eur. J.* **2009**, *15*, 3661.
(13) (a) Wang, S.; Ferbinteanu, M.; Yamashita, M. *Inorg. Chem.* **2007**, *46*, 610. (b) Kwak, H. Y.; Ryu, D. W.; Kim, H. C.; Koh, E. K.; Cho, B. K.; Hong, C. S. *Dalton. Trans.* **2009**, 1954. (c) Wen, H.-R.; Tang, Y.-Z.; Liu, C.-M.; Chen, J.-L.; Yu, C.-L. *Inorg. Chem.* **2009**, *48*, 10177. (d) Wang, S.; Ferbinteanu, M.; Yamashita, M. *Solid State Sci.* **2008**, *10*, 915.
(14) Kim, J. I.; Yoon, J. H.; Kwak, H. Y.; Koh, E. K.; Hong, C. S. *Eur. J. Inorg. Chem.* **2008**, 2756.
(15) Karmakar, R.; Choudhury, C. R.; Bravic, G.; Sutter, J.-P.; Mitra, S. *Polyhedron* **2004**, *23*, 949.

Table 1. Crystallographic Data for **1**−**5**

	1	**2**	**3**	**4**	**5**
formula	$C_{38}H_{39}BFeMnN_{12}O_7$	$C_{32}H_{29}BCl_2FeMnN_{11}O_3$	$C_{40}H_{40}BFeMnN_{11}O_4$	$C_{30}H_{30}BFeMnN_{11}O_5$	$C_{38}H_{32}BFeMnN_{11}O_2$
formula weight	897.41	808.16	860.43	746.25	796.35
crystal system	momoclinic	monoclinic	monoclinic	triclinic	monoclinic
space group	$C2/c$	$P2_1/c$	$P2_1/n$	$P\bar{1}$	$P2_1/c$
temperature (K)	130	293	293	293	293
a (Å)	19.6777(3)	16.7206(5)	14.2604(3)	12.4979(6)	12.3691(17)
b (Å)	14.2830(2)	14.4747(4)	17.9056(4)	13.0039(7)	14.118(2)
c (Å)	30.1632(4)	17.4021(5)	17.3380(4)	13.8787(12)	23.229(3)
α (deg)				113.551(3)	
β (deg)	108.1790(10)	109.396(2)	111.912(1)	107.610(2)	91.595(5)
γ (deg)				102.448(2)	
V(Å^3)	8054.4	3972.7(2)	4107.28(16)	1818.8(2)	4054.8(10)
Z	8	4	4	2	4
d_{calc} (g cm^{-3})	1.480	1.351	1.391	1.363	1.304
μ (mm^{-1})	0.739	0.863	0.716	0.798	0.716
F(000)	3704	1648	1780	766	1636
reflections collected	32831	39977	39953	30083	41750
unique reflections	10047	9831	10191	8662	10055
goodness-of-fit	1.020	0.896	1.014	0.933	1.041
R1[a] [$I > 2\sigma(I)$]	0.0446	0.0667	0.0615	0.0696	0.0722
wR2[b] [$I > 2\sigma(I)$]	0.1120	0.1303	0.1333	0.1767	0.1660

[a] $R1 = \sum||F_o| - |F_c||/\sum|F_o|$. [b] $wR2 = [\sum w(F_o^2 - F_c^2)^2/\sum w(F_o^2)^2]^{1/2}$.

in the dark, producing brown crystals in 52% yield. Anal. Calcd for $C_{32}H_{29}BCl_2FeMnN_{11}O_3$: C, 47.56; H, 3.62; N, 19.07. Found: C, 47.67; H, 3.72; N, 18.85.

[(Tp)Fe(CN)$_3$][Mn(2-acnapen)(MeOH)]·MeOH (3). [Mn(2-acnapen)(H_2O)]Cl (0.10 mmol) was dissolved in MeOH (10 mL), and (Ph_4P)[(Tp)Fe(CN)$_3$]·H_2O (0.10 mmol) was dissolved in H_2O/MeCN (1:1 v/v, 10 mL). Both solutions were mixed together and stirred for 3 min. The resultant solution was filtered, slowly evaporated in the dark, which yielded brown crystals in 60% yield. The MeOH molecules were replaced by water molecules in air. The hydrated sample was checked by elemental analysis. Anal. Calcd for $C_{38}H_{36}BFeMnN_{11}O_4$: C, 54.83; H, 4.36; N, 18.51. Found: C, 54.45; H, 3.99; N, 18.18.

[(Tp)Fe(CN)$_3$][Mn(3-MeOsalen)(H_2O)] (4). A solution of [Mn(3-MeOsalen)(H_2O)]ClO_4 (0.10 mmol) in MeOH/MeCN (1:1 v/v, 10 mL) was reacted with a solution of (Ph_4P)[(Tp)Fe(CN)$_3$]·H_2O (0.10 mmol) in MeCN (10 mL) for 3 min. The resulting solution was then filtered and slowly evaporated in the dark, which gave brown crystals in 40% yield. Anal. Calcd for $C_{30}H_{30}BFeMnN_{11}O_5$: C, 48.29; H, 4.05; N, 20.65. Found: C, 48.40; H, 4.29; N, 20.17.

[(Tp)Fe(CN)$_3$][Mn(2-acnapen)]·H_2O (5). A solution of [Mn(2-acnapen)(H_2O)]Cl (0.10 mmol) in H_2O/MeCN (1:1 v/v, 10 mL) was treated with a solution of (Ph_4P)[(Tp)Fe(CN)$_3$]·H_2O (0.10 mmol) in MeCN (10 mL). Stirring of the solution for 3 min, it was filtered, slowly evaporated in the dark, precipitating brown crystals in 40% yield. Anal. Calcd for $C_{38}H_{34}BFeMnN_{11}O_3$: C, 56.05; H, 4.21; N, 18.92. Found: C, 55.96; H, 4.05; N, 18.71.

Physical Measurements. Elemental analyses for C, H, and N were performed at the Elemental Analysis Service Center of Sogang University. Infrared spectra were obtained from KBr pellets with a Bomen MB-104 spectrometer. Magnetic susceptibilities for **1**−**5** were carried out using a Quantum Design SQUID (dc) and a PPMS (ac) susceptometer. Diamagnetic corrections of **1**−**5** were estimated from Pascal's Tables.

Crystallographic Structure Determination. X-ray data for **1**−**5** were collected on a Bruker SMART APEXII diffractometer equipped with graphite monochromated MoKα radiation (λ = 0.71073 Å). Preliminary orientation matrix and cell parameters were determined from three sets of ω/ϕ (**1**−**3**) and ω scans (**4** and **5**) at different starting angles. Data frames were obtained at scan intervals of 0.5° with an exposure time of 10 s per frame. The reflection data were corrected for Lorentz and polarization factors. Absorption corrections were carried out using SADABS.[16] The structures were solved by direct methods and refined by full-matrix least-squares analysis using anisotropic thermal parameters for non-hydrogen atoms with the SHELXTL program.[17] Lattice solvent molecules in **2**, **4**, and **5** are significantly disordered and could not be modeled properly, thus the program SQUEEZE,[18] a part of the PLATON package[19] of crystallographic software, was used to calculate the solvent disorder area and remove its contribution to the overall intensity data. All hydrogen atoms except for hydrogens bound to water molecules were calculated at idealized positions and refined with the riding models.

Computational Details. DFT calculations based on the crystallographic coordinates were carried out using the unrestricted B3LYP functional[20] implemented in Gaussian 03.[21] The 6-311G* basis set[22] is used for the metal ions and the bound atoms, and the 6-31G basis set[23] is taken for the other atoms.[13a]

(16) Sheldrick, G. M.*SADABS, A program for area detector absorption corrections*; University of Göttingen: Göttingen, Germany, 1994.
(17) Sheldrick, G. M. *SHELXTL*, version 5; Bruker AXS: Madison, WI, 1995.
(18) van der Sluis, P.; Spek, A. L. *Acta Crystallogr.* **1990**, *A46*, 194.
(19) Spek, A. L. *Acta Crystallogr.* **1990**, *A46*, 1.
(20) (a) Becke, A. D. *Phys. Rev. A* **1988**, *38*, 3098. (b) Lee, C. T.; Yang, W. T.; Parr, R. G. *Phys. Rev. B* **1988**, *37*, 785. (c) Stephens, P. J.; Devlin, F. J.; Chabalowski, C. F.; Frisch, M. J. *J. Phys. Chem.* **1994**, *98*, 11623.
(21) Frisch, M. J.; Trucks, G. W.; Schlegel, H. B.; Scuseria, G. E.; Robb, M. A.; Cheeseman, J. R.; Montgomery, Jr., J. A.; Vreven, T.; Kudin, K. N. ; Burant, J. C. ; Millam, J. M.; Iyengar, S. S.; Tomasi, J.; Barone, V.; Mennucci, B.; Cossi, M.; Scalmani, G.; Rega, N.; Petersson, G. A.; Nakatsuji, H.; Hada, M.; Ehara, M.; Toyota, K.; Fukuda, R.; Hasegawa, J.; Ishida, M.; Nakajima, T.; Honda, Y.; Kitao, O.; Nakai, H.; Klene, M.; Li, X.; Knox, J. E. ; Hratchian, H. P. ; Cross, J. B.; Bakken, V.; Adamo, C.; Jaramillo, J.; Gomperts, R.; Stratmann, R. E.; Yazyev, O.; Austin, A. J. ; Cammi, R.; Pomelli, C.; Ochterski, J. W.; Ayala, P. Y. ; Morokuma, K.; Voth, G. A. ; Salvador, P.; Dannenberg, J. J.; Zakrzewski, V. G. ; Dapprich, S.; Daniels, A. D. ; Strain, M. C.; Farkas, O.; Malick, D. K. ; Rabuck, A. D.; Raghavachari, K.; Foresman, J. B. ; Ortiz, J. V. ; Cui, Q.; Baboul, A. G. ; Clifford, S.; Cioslowski, J.; Stefanov, B. B.; Liu, G. ; Liashenko, A.; Piskorz, P.; Komaromi, I.; Martin, R. L. ; Fox, D. J. ; Keith, T.; Al-Laham, M. A.; Peng, C. Y. ; Nanayakkara, A.; Challacombe, M.; Gill, P. M. W.; Johnson, B.; Chen, W.; Wong, M. W. ; Gonzalez, C.; Pople, J. A. *Gaussian 03*, Revision D.02; Gaussian, Inc.: Wallingford, CT, 2004.
(22) (a) Krishnan, R.; Binkley, J. S.; Seeger, R.; Pople, J. A. *J. Chem. Phys.* **1980**, *72*, 650. (b) McLean, A. D.; Chandler, G. S. *J. Chem. Phys.* **1980**, *72*, 5639.
(23) (a) Hehre, W. J.; Ditchfield, R.; Pople, J. A. *J. Chem. Phys.* **1972**, *56*, 2257. (b) Hariharan, P. C.; Pople, J. A. *Theor. Chim. Acta* **1973**, *28*, 213.

To evaluate exchange coupling constants, the high-spin (HS) state (sextet for $Fe^{III}-Mn^{III}$ dimer) and the broken-symmetry (BS) calculations employing guess functions generated with Gaussian 09 were separately performed. The exchange coupling constant on the basis of the spin Hamiltonian ($H = -JS_1 \cdot S_2$) is calculated with $E_{HS} - E_{BS} = -J(2S_1S_2 + S_2)$ where S_1 and S_2 stand for the total theoretical spin states of the heterometal centers assuming $S_1 > S_2$.[24]

Results and Discussion

Synthesis and Characterization. The $[(Tp)Fe(CN)_3]^-$ precursor was reacted with the Mn(III) Schiff bases, yielding crystalline brown solids. Notably, the use of a Mn complex chelated with 2-acnapen in the reaction afforded a dimeric molecule (**3**) in H_2O/MeCN/MeOH and a 1D zigzag chain structure (**5**) in H_2O/MeCN. Compared with **5**, the dimeric unit (**3**) was stabilized in the presence of MeOH, indicating that the structural evolution toward higher dimensionality is blocked by the coordinative MeOH molecules in this case. Thus, choice of solvents in reaction systems plays an important role in engendering different structural patterns.[25] The peculiar CN stretching vibrations allow us to elucidate coordination of CN ligands to neighboring metal ions. In reference to the CN peak evident at 2123 m cm^{-1} for $[Ph_4P][(Tp)Fe(CN)_3]$, the CN bands are observed at 2131 m cm^{-1} for **1**, 2131w cm^{-1} for **2**, 2135 m and 2143 m cm^{-1} for **3**, 2123 m, 2129 m, and 2137 m (sh) cm^{-1} for **4**, and 2115 w, 2129 m, and 2137 m cm^{-1} for **5**. The shift of some CN vibrations toward higher frequencies is indicative of the occurrence of bridging mode of CN ligands.[26]

Description of the Structures. The structures of **1**−**5** have been characterized using single crystal X-ray diffraction techniques. Crystallographic data and the details of data collection for all the complexes are listed in Table 1, and selected bond lengths and angles for **1**−**5** are summarized in Table 2.

Complexes 1−**4.** The crystal structures of dimeric complexes **1**−**4** are depicted in Figure 1 with the selected atom-labeling schemes. The anionic precursor $[(Tp)Fe(CN)_3]^-$ and the cationic Mn Schiff bases in the structures are linked together through a single CN bridge. The dimeric moiety is completed by the coordination of a water or a methanol molecule to one of the axial sites of the Mn Schiff base. Each Fe center adopts a distorted octahedral geometry consisting of three N atoms from Tp and three C atoms from CN ligands. One of three CN groups participates in additional binding to an adjacent Mn ion and the other CN ligands remain unbound. The average Fe−C bond lengths are similar, 1.924(4) Å for **1**, 1.933(8) Å for **2**, 1.926(12) Å for **3**, and 1.916(1) Å for **4**. The Fe−C−N angle is deviated from 180°, being 5.0° in maximum for **1**, 2.9° for **2**, 2.5° for **3**, and 3.0° for **4**. The Mn environment is best described as a Jahn−Teller distorted octahedron comprising the equatorial short Mn−N(O) bond lengths [mean $Mn-N(O)_{eq}$ = 1.93(5) Å for **1**, 1.93(7) Å for **2**, 1.94(7) Å for **3**, and 1.92(5) Å for **4**] and the apical long Mn−N distances [$Mn1-N_{ax}$ = 2.334(2) Å for **1**, 2.307(4) Å for **2**, 2.247(3) Å for **3**, and 2.298(4) Å for **4**; $Mn1-O_{ax}$ = 2.278(2) Å for **1**, 2.293(3) Å for **2**, 2.252(3) Å for **3**, and 2.340(3) Å for **4**]. The Mn−N−C angles in the bridging pathways are 156.31(19)° for **1**, 157.7(4)° for **2**, 159.0(3)° for **3**, and 163.8(4)° for **4**, which are magnetically important. The intradimer distances between Fe and Mn centers are 5.283 Å for **1**, 5.228 Å for **2**, 5.211 Å for **3**, and 5.298 Å for **4**.

In the extended structure of **1** (Figure 2), extensive $\pi-\pi$ interactions between naphthalene rings with centroid distances of 3.536 and 3.534 Å occur where the intermolecular Mn1−Mn1 separation is 7.868 Å. The correlated dimer of dimers through the intermolecular contacts

Table 2. Selected Bond Lengths (Å) and Angles (deg) for **1**−**5**

		1	
Fe(1)−C(3)	1.920(2)	Fe(1)−C(1)	1.926(2)
Fe(1)−C(2)	1.927(2)	Fe(1)−N(4)	1.969(2)
Fe(1)−N(5)	1.9757(19)	Fe(1)−N(6)	1.9862(19)
N(1)−Mn(1)	2.334(2)	Mn(1)−O(2)	1.8792(18)
Mn(1)−O(1)	1.8958(16)	Mn(1)−N(11)	1.965(2)
Mn(1)−N(10)	1.974(2)	Mn(1)−O(3)	2.2780(17)
N(1)−C(1)−Fe(1)	176.8(2)	C(1)−N(1)−Mn(1)	156.31(19)
N(2)−C(2)−Fe(1)	176.8(2)	N(3)−C(3)−Fe(1)	175.0(2)
		2	
Fe(1)−C(1)	1.925(5)	Fe(1)−C(2)	1.934(6)
Fe(1)−C(3)	1.941(4)	Fe(1)−N(8)	1.964(4)
Fe(1)−N(4)	1.974(3)	Fe(1)−N(6)	1.987(4)
N(1)−Mn(1)	2.307(4)	Mn(1)−O(2)	1.860(3)
Mn(1)−O(1)	1.880(3)	Mn(1)−N(11)	1.980(3)
Mn(1)−N(10)	1.990(4)	Mn(1)−O(3)	2.293(3)
N(1)−C(1)−Fe(1)	178.4(4)	C(1)−N(1)−Mn(1)	157.7(4)
N(2)−C(2)−Fe(1)	178.1(4)	N(3)−C(3)−Fe(1)	177.1(4)
		3	
Fe(1)−C(1)	1.912(4)	Fe(1)−C(2)	1.929(4)
Fe(1)−C(3)	1.936(4)	Fe(1)−N(4)	1.972(3)
Fe(1)−N(6)	1.981(3)	Fe(1)−N(8)	1.982(3)
N(1)−Mn(1)	2.247(3)	Mn(1)−O(2)	1.878(3)
Mn(1)−O(1)	1.880(3)	Mn(1)−N(11)	1.991(3)
Mn(1)−N(10)	1.994(3)	Mn(1)−O(3)	2.252(3)
N(1)−C(1)−Fe(1)	177.5(3)	C(1)−N(1)−Mn(1)	159.0(3)
N(2)−C(2)−Fe(1)	178.1(4)	N(3)−C(3)−Fe(1)	177.7(4)
		4	
Fe(1)−C(1)	1.915(5)	Fe(1)−C(2)	1.916(5)
Fe(1)−C(3)	1.917(6)	Fe(1)−N(6)	1.966(4)
Fe(1)−N(4)	1.980(4)	Fe(1)−N(8)	1.982(4)
Mn(1)−O(1)	1.870(3)	Mn(1)−O(2)	1.882(3)
Mn(1)−N(10)	1.955(4)	Mn(1)−N(11)	1.978(5)
Mn(1)−N(1)	2.298(4)	Mn(1)−O(5)	2.340(3)
N(1)−C(1)−Fe(1)	177.0(5)	N(2)−C(2)−Fe(1)	177.8(5)
C(1)−N(1)−Mn(1)	163.8(4)	N(3)−C(3)−Fe(1)	178.7(5)
		5	
Fe(1)−C(3)	1.913(4)	Fe(1)−C(2)	1.923(4)
Fe(1)−C(1)	1.930(4)	Fe(1)−N(6)	1.965(3)
Fe(1)−N(8)	1.967(3)	Fe(1)−N(4)	1.990(3)
N(1)−Mn(1)	2.372(3)	N(3)−Mn(1)b	2.322(3)
N(10)−Mn(1)	1.967(4)	Mn(1)−O(2)	1.868(3)
Mn(1)−O(1)	1.873(2)	Mn(1)−N(11)	1.990(3)
Mn(1)−N(3)a	2.322(3)		
N(1)−C(1)−Fe(1)	173.2(3)	C(1)−N(1)−Mn(1)	149.3(3)
N(2)−C(2)−Fe(1)	178.5(4)	N(3)−C(3)−Fe(1)	177.6(3)
C(3)−N(3)−Mn(1)b	148.7(3)		

(24) Ruiz, E.; Cano, J.; Alvarez, S.; Alemany, P. *J. Comput. Chem.* **1999**, *20*, 1391.

(25) Wang, X.-Y.; Wang, L.; Wang, Z.-M.; Gao, S. *J. Am. Chem. Soc.* **2006**, *128*, 674.

(26) Dunbar, K. R.; Heintz, R. A. *Prog. Inorg. Chem.* **1997**, *45*, 283.

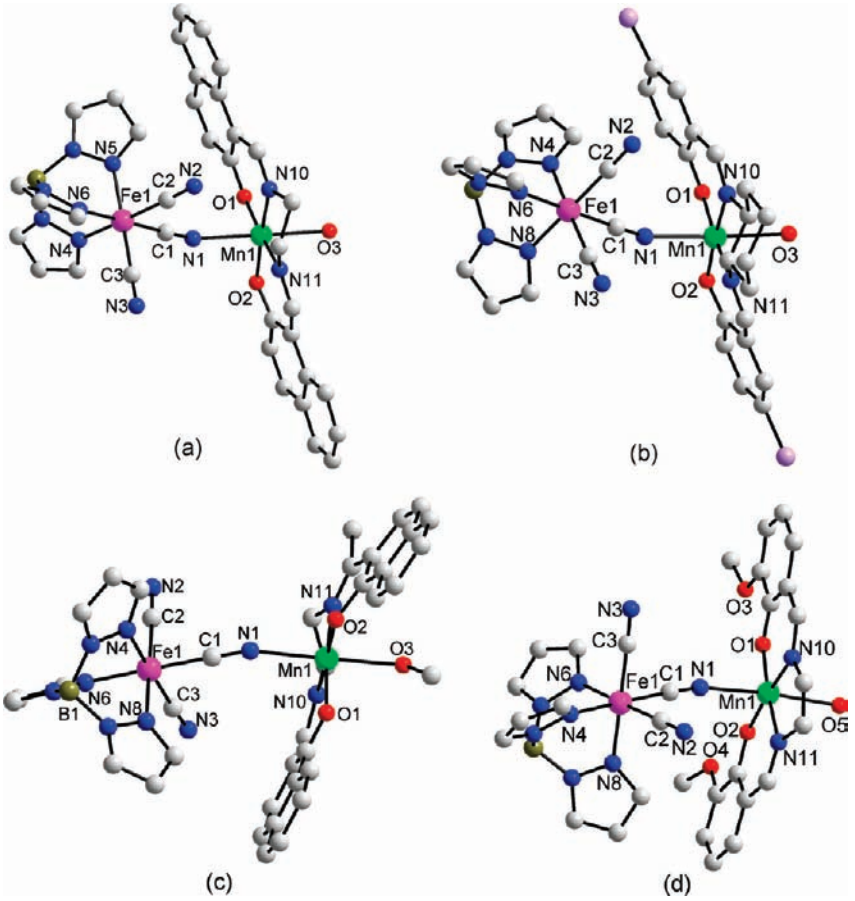

Figure 1. Molecular views of (a) **1**, (b) **2**, (c) **3**, and (d) **4** with the selected atom-labeling schemes. The colors represent Fe in pink, Mn in green, N in blue, O in red, B in brown, and C in gray.

propagate further with additional $\pi-\pi$ stackings between benzene rings (centroid distances = 3.685 and 3.730 Å; interdimer Mn1−Mn1 distances = 7.894 and 7.903 Å, respectively). Interestingly, CH$-\pi$ interactions between pyrazole hydrogens and benzene rings (distance = 2.658 Å) reside within a dimeric unit.[27] Furthermore, pyrazole rings are stacked with a distance of 3.526 Å, and the intermolecular Fe1−Fe1 distance is 8.063 Å. The N atoms of unbound CN groups form hydrogen bonding to lattice water molecules (N2−Ow = 2.942 Å, N3−Ow = 2.817 Å), which are further hydrogen-bonded to axially coordinated water molecules (Ow−O3 = 2.698 and 2.825 Å). Overall, such multiple intermolecular contacts lead to the construction of a complicated three-dimensional (3D) architecture.

The extended molecular view of **2** (Figure 3) shows that water molecules (O3) and phenoxide oxygens (O1) are doubly hydrogen-bonded to confer a dimer of dimers (O1−O3 = 2.825 Å). At the same time, there are intramolecular $\pi-\pi$ interactions between benzene rings of 5-Clsalcy (centroid distance = 3.739 Å). The Mn−Mn distance through these noncovalent bonds is 5.056 Å. The structure is expanded toward a 1D chain with assistance of CH$-\pi$ interactions between pyrazole rings of Tp ligands and benzene rings (distance = 2.643 Å).[27]

As shown in Figure 4, two types of intermolecular $\pi-\pi$ contacts between pyrzaole rings of Tp ligands (centroid distances = 3.646 and 3.971 Å) are found in **3**, and the Fe−Fe distances via the contacts are 7.868 and 7.981 Å, respectively. One (N3) of two free CN groups of the Fe tricyanide and a coordinate water molecule (O3) constitute hydrogen bonding (N3−O3 = 2.769 Å) with an intermolecular Fe−Mn distance of 7.006 Å. All the intermolecular stackings bring about the building of a 3D network structure.

For **4** (Figure 5), axial water molecules bound to Mn ions are subject to quadruple hydrogen bonds among phenoxide oxygens and methoxy oxygens of 3-Meosalen, resulting in a dimer of dimers. The hydrogen bond lengths range from 2.898 Å to 2.940 Å. Additional $\pi-\pi$ interactions between benzene rings (centroid distance = 3.939 Å) coexist, and the interdimer Mn−Mn distance is 4.868 Å. The dimer of dimers are correlated through extra $\pi-\pi$ interactions between pyrazole rings of Tp ligands (centroid distance = 3.554 Å, intermolecular Fe−Fe distance = 7.573 Å), giving rise to a 1D structure.

Complex 5. The structure of **5** is made up of the *facial* Fe tricyanide precursor and the $[Mn(2\text{-acnapen})]^+$ moiety (Figure 6). A zigzag 1D chain is organized in a way that two CN ligands of Tp link adjacent $Mn(L)^+$ moieties. In the Fe side, the average Fe−C bond length is 1.922(9) Å and the maximal deviation of the Fe−C−N angle from linearity is 6.8°. A significant Jahn−Teller tetragonal elongation around a Mn center emerges as judged by the equatorial short Mn−N(O) bond lengths [mean Mn−N(O) = 1.93(6) Å] and the apical long Mn−N distances

(27) Hong, C. S.; Yoon, J. H.; Lim, J. H.; Ko, H. H. *Eur. J. Inorg. Chem.* **2005**, 4818.

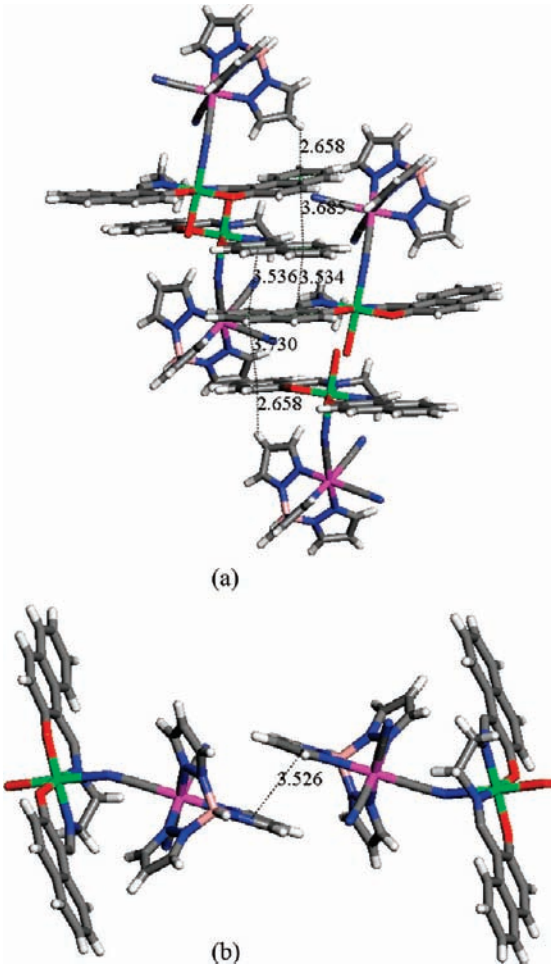

Figure 2. Extended structure of **1** formed by $\pi-\pi$ contacts and CH$-\pi$ interactions.

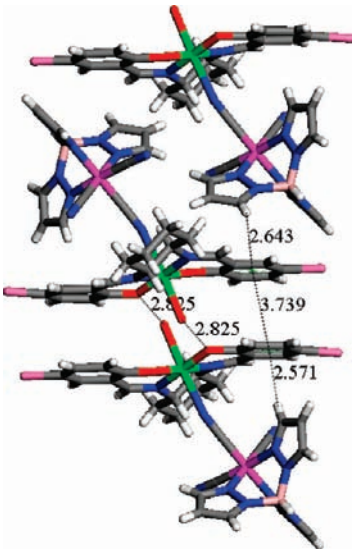

Figure 3. Extended structure of **2** displaying $\pi-\pi$ contacts and CH$-\pi$ interactions.

[Mn1$-$N1 = 2.372(3) and Mn1b$-$N3 = 2.322(3) Å; b = $1-x, 0.5+y, 0.5-z$]. The Mn$-$N$-$C angles are 149.3(3)° for Mn1$-$N1$-$C1 and 148.7(3)° for Mn1b$-$N3$-$C3. The intrachain Fe$-$Mn distances are 5.203 Å for Fe1$-$Mn1 and 5.185 Å for Fe1$-$Mn1b. In contrast to the dimeric systems, complex **5** has no $\pi-\pi$ stacking interactions between chains (Supporting Information, Figure S1). The shortest interchain Fe$-$Mn distance is 9.187 Å.

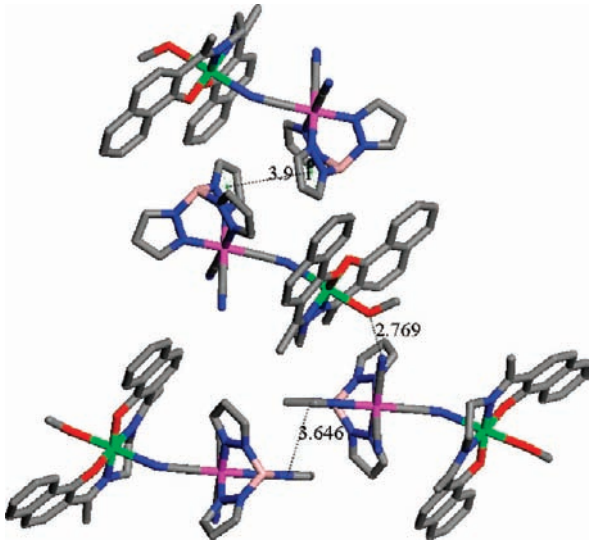

Figure 4. Extended structure of **3** showing $\pi-\pi$ contacts and hydrogen bonds.

Magnetic Properties of 1. The magnetic susceptibility data per FeMn of **1** were collected at a field of 1000 G and temperatures of 2$-$300 K, as seen in Figure 7. The $\chi_m T$ value at 300 K is equal to 4.23 cm^3 K mol^{-1}, which is larger than the spin-only one (3.38 cm^3 K mol^{-1}) anticipated from noncoupled one Fe^{III} ($S_{Fe} = 1/2$) and one Mn^{III} spins ($S_{Mn} = 2$). It is mentioned that the approximate point group of [Fe(Tp)(CN)$_3$]$^-$ is C_{3v}, and in the C_{3v} FeN$_3$(CN)$_3$ coordination compressed along the trigonal axis the orbital ground state is doubly degenerate. In this case, the orbital moment of Fe(III) is unquenched and is coupled with spin via spin$-$orbit coupling.[28] This contribution may be responsible for the observed high $\chi_m T$ value. As the temperature is lowered, $\chi_m T$ increases gradually and then abruptly, reaching a value of 5.92 cm^3 K mol^{-1} at 6 K. Below the cusp temperature (T_{max}), a sharp drop in $\chi_m T$ is obviously observed. The rise in the $\chi_m T(T)$ plot indicates the presence of intradimer ferromagnetic interactions through the CN linkage, and the decrease below T_{max} may originate from zero-field splitting of the molecule.

Employing a dinuclear magnetic model with the spin Hamiltonian $H = -JS_{Mn} \cdot S_{Fe}$ under consideration of the intermolecular interactions (zJ'), we fitted the experimental data ($T > 6$ K) to the equation below.

$$\chi = (Ng^2\beta^2/3kT)[A/B] \qquad (1)$$

$$A = 15 + 52.5\exp(2.5x), \quad B = 4 + 6\exp(2.5x),$$
$$x = J/kT$$

$$\chi_m = \chi/(1 - zJ'\chi/Ng^2\beta^2)$$

A fitted result is $g = 2.19$, $J = 7.48$ cm^{-1}, and $zJ' = 0.19$ cm^{-1}. From the magnetic parameters, it is manifest that

(28) Atanasov, M.; Comba, P.; Daul, C. A. *Inorg. Chem.* **2008**, *47*, 2449.

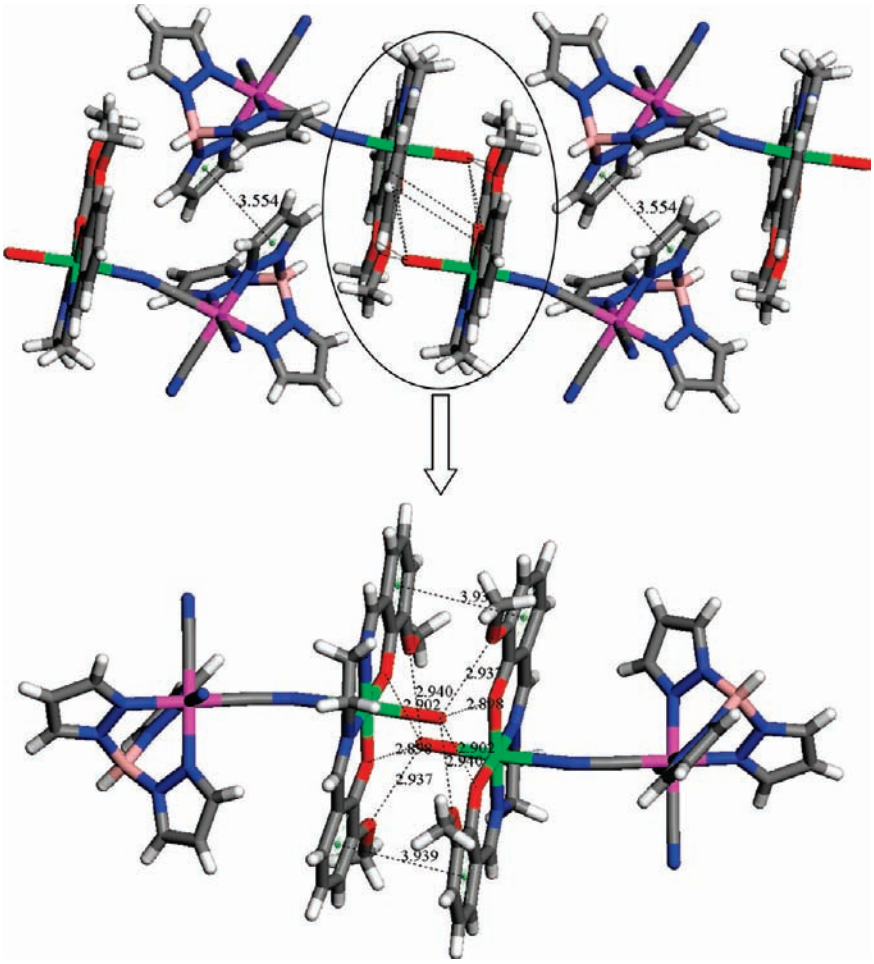

Figure 5. Extended structure of **4** including $\pi-\pi$ contacts and hydrogen bonds.

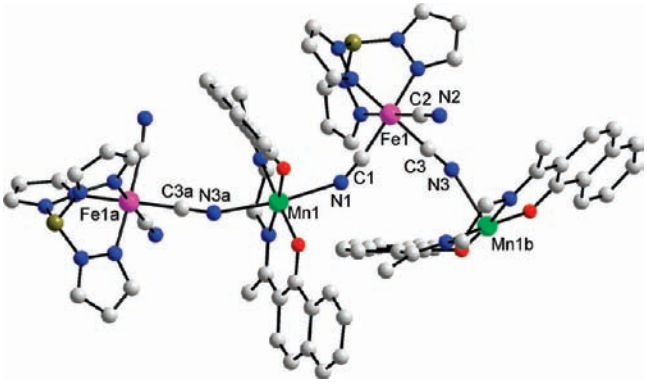

Figure 6. Molecular view of **5** with the selected atom-labeling scheme. Symmetry transformations used to generate equivalent atoms: a $= -x+1$, $y-0.5, -z+0.5$; b $= -x+1, y+0.5, -z+0.5$.

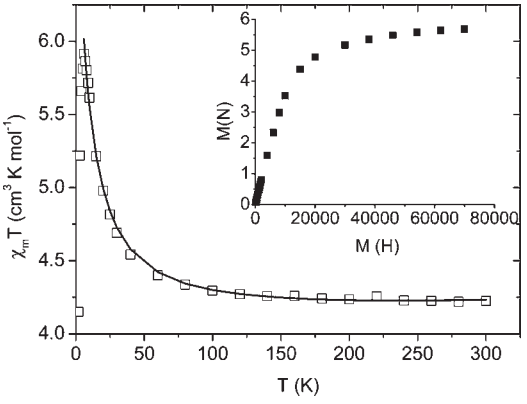

Figure 7. Plots of $\chi_m T$ vs T at 0.1 T (main panel) and magnetization vs H at 2 K (inset) for **1**. The solid line in the main panel represents the computed curve.

ferromagnetic interactions between Mn(III) and Fe(III) are mediated by the CN bridge. The resultant J value is similar to those of most bimetallic $Fe^{III}Mn^{III}$ compounds based on the same *fac*-Fe tricyanide,[13] and these magnetic traits are, however, contrary to $Fe^{III}Mn^{III}$ families with *mer*-Fe tricyanides where antiferromagnetic properties are dominantly detected.[8−10] The $M(H)$ curve demonstrates that the magnetization value is saturated at 5.69 $N\beta$ at 7 T, which is slightly larger than the theoretical value calculated from $g(S_{Mn} + S_{Fe})$ with $g = 2.19$.

Magnetic Properties of 2. The temperature dependence of magnetic data for **2** is plotted in Figure 8, measured at 0.1 T and the temperature range of 2−300 K. The $\chi_m T$ value is 4.09 cm^3 K mol^{-1} at 300 K, a little larger than the expected value for independent Mn(III) and Fe(III) spins assuming $g = 2$. A gradual increase in $\chi_m T$ is encountered on cooling, and a maximum of 4.25 cm^3 K mol^{-1} at 20 K is reached. This general trend in $\chi_m T$ again evidences the operation of ferromagnetic couplings among magnetic centers. A sharp downturn in the $\chi_m T$ versus T graph is

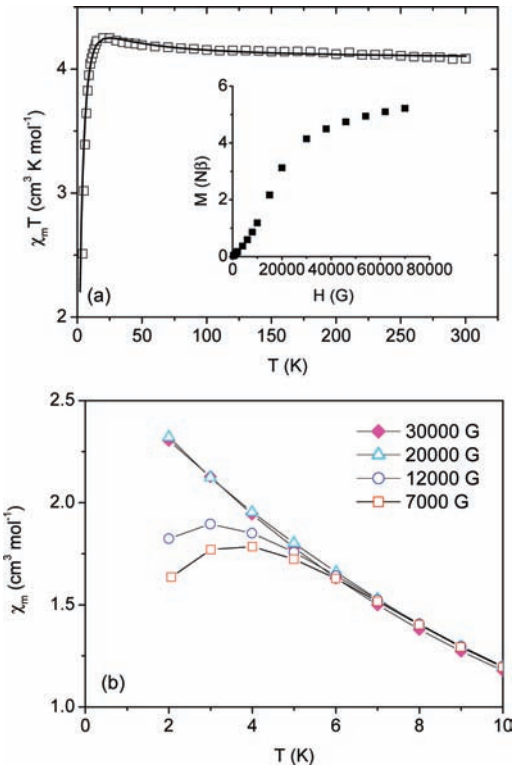

Figure 8. (a) Plots of $\chi_m T$ vs T at 0.1 T in the main panel and magnetization vs H at 2 K in the inset for **2**. The solid line stands for the fitted curve. (b) Plots of χ_m vs T at indicated fields for **2**.

found right below the maximum temperature, which is associated with zero-field splitting and/or intermolecular antiferromagnetic interactions.

The magnetic exchange coupling constant in **2** was assayed by applying the dinuclear eq 1. A best fit affords parameters of $g = 2.20$, $J = 6.66\ \text{cm}^{-1}$, and $zJ' = -0.67\ \text{cm}^{-1}$. The magnetic data in the whole temperature range are well reproduced with these values. The positive J constant designates that ferromagnetic interactions within a dinuclear unit are operative through the bridging CN group. The interdimer antiferromagnetic interactions (zJ') can be communicated through double hydrogen bonds between phenoxide oxygens and coordinate water molecules because the shortest interdimer M−M distance of 5.056 Å is relevant to the noncovalent contacts (Figure 3). In the $M(H)$ data, the S-shaped curve arrives at a saturation magnetization of 5.22 $N\beta$, which approaches the calculated one from S_{Mn} and S_{Fe} with $g = 2.2$. The derivative of $M(H)$ against H has a peak at $H_C = 15$ kG. As illustrated in Figure 8(b), the field-cooled magnetizations clearly reveal a magnetic phase transition below and above H_C. It appears that the weak interdimer antiferromagnetic interactions are overcome by the external magnetic field above H_C and all spins are aligned in the field direction. This feature can be understood in terms of a field-induced spin-flop-like transition from the antiferromagnetic state among dimers to a paramagnetic phase. The similar phenomenon

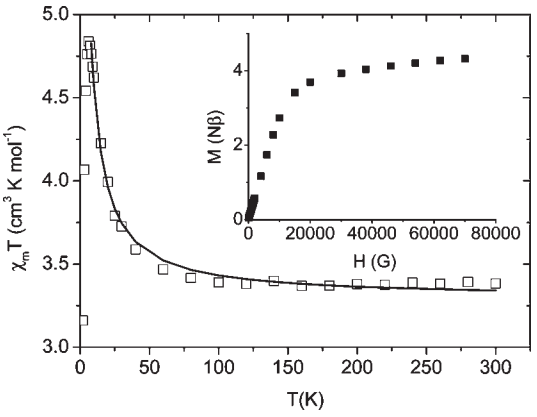

Figure 9. Plots of $\chi_m T$ vs T at 0.1 T (main panel) and magnetization vs H at 2 K (inset) for **3**. The solid line gives the fitted curve.

was also found in magnetic assemblies connected by diverse bridges such as cyanide-, carboxylate-, or azide.[29]

Magnetic Properties of 3. The cryomagnetic data for **3** are plotted in Figure 9. For **3**, $\chi_m T$ at 300 K is equal to 3.38 cm^3 K mol^{-1}, in good agreement with the expected spin-only value from noncoupled Fe^{III} ($S_{Fe} = 1/2$) and Mn^{III} ($S_{Mn} = 2$). As the temperature is lowered, $\chi_m T$ increases gradually and amounts to a maximum of 4.84 cm^3 K mol^{-1} at 6 K. This behavior is in concert with the presence of ferromagnetic couplings between magnetic centers. An abrupt drop below 6 K is attributable to zero-field splitting of a ground state.

The magnetic exchange coupling constant of **3** was obtained using the same dinuclear model. A best fit to the experimental data gives $g = 1.98$, $J = 4.91\ \text{cm}^{-1}$, and $zJ' = 0.30\ \text{cm}^{-1}$. Like **1** and **2**, intradimer ferromagnetic couplings are transmitted by the CN bridge. In the $M(H)$ curve, the saturation magnetization value corresponds to 4.32 $N\beta$, close to the theoretical one anticipated from the ferromagnetic consequence of $g(S_{Mn}+S_{Fe})$. A small discrepancy between experimental and theoretical values arises from the magnetic anisotropy of the dimer.

Magnetic Properties of 4. The temperature dependence of the magnetic susceptibility was recorded at $H = 0.1$ T and $T = 2-300$ K (Figure 10). The $\chi_m T$ value of 3.49 cm^3 K mol^{-1} at 300 K is somewhat smaller than the theoretical value for noninteracting Mn(III) and Fe(III) ions with $g = 2$. Decreasing the temperature causes $\chi_m T$ to undergo a continuous reduction and then a drastic drop. It is noteworthy that this behavior definitely represents the existence of antiferromagnetic interactions among Mn(III) and Fe(III) centers, which is in conflict with the magnetic properties observed in **1**−**3**.

To probe the magnetic exchange coupling constant between paramagnetic centers we used the dinuclear magnetic model again. A least-squares fit yields $g = 2.02$, $J = -1.40$ cm^{-1}, and $zJ' = -0.13\ \text{cm}^{-1}$. The negative J value stands for intradinuclear antiferromagnetic arrangements exchanged via the CN bridge, which is opposite to the other Fe(III)−Mn(III) dimers of **1**−**3**. The field-dependent magnetization at 2 K was measured in $H = 0-7$ T, as shown in the inset of Figure 10. The characteristic sigmoidal curve is observed, and it is related to a field-induced magnetic phase transition.[29] The critical field of $H_C = 15$ kG is taken by the peak of dM/dH. At 7 T, the magnetization is saturated at 4.41 $N\beta$ at 7 T, which is similar to $g(S_{Mn}+S_{Fe})$ with

(29) (a) Hu, K.-L.; Kurmoo, M.; Wang, Z.; Gao, S. *Chem.—Eur. J.* **2009**, *15*, 12050. (b) Li, W.; Ju, Z.-F.; Yao, Q.-X.; Zhang, J. *CrystEngComm* **2008**, *10*, 1325. (c) Ko, H. H.; Lim, J. H.; Yoo, H. S.; Kang, J. S.; Kim, H. C.; Koh, E. K.; Hong, C. S. *Dalton Trans.* **2007**, 2061. (d) Yoon, J. H.; Yoo, H. S.; Kim, H. C.; Yoon, S. W.; Suh, B. J.; Hong, C. S. *Inorg. Chem.* **2009**, *48*, 816. (e) You, Y. S.; Yoon, J. H.; Kim, H. C.; Hong, C. S. *Chem. Commun.* **2005**, 4116.

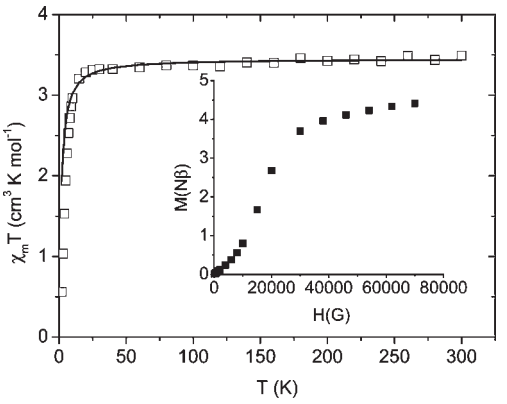

Figure 10. Plots of $\chi_m T$ vs T at 0.1 T (main panel) and magnetization vs H at 2 K (inset) for **4**. The solid line denotes the fitted curve.

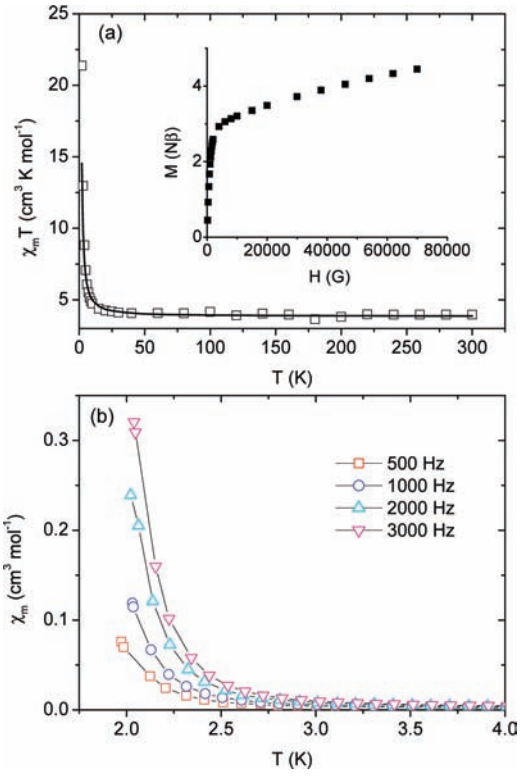

Figure 11. (a) Plots of $\chi_m T$ vs T at 0.1 T (main panel) and magnetization vs H at 2 K (inset) for **5**. The solid line denotes the fitted curve. (b) Plot of out-of-phase (χ_m'') component of ac magnetic susceptibility data for **5**.

$g = 2.02$. From the $M(H)$ data, we conclude that the antiferromagnetic coupings within a dimer and between dimers are destroyed by the application of a magnetic field ($H > H_C$) and that all spins are oriented along the field direction.

Magnetic Properties of 5. Figure 11(a) shows the temperature dependence of magnetic data at $H = 0.1$ T and $T = 2-300$ K. The room-temperature $\chi_m T$ is 3.96 cm^3 K mol^{-1}, which is consistent with the predicted spin-only value from noncoupled Fe^{III} ($S_{Fe} = 1/2$) and Mn^{III} ($S_{Mn} = 2$) spins. The $\chi_m T$ product increases steadily and then dramatically, attaining a value of 21.37 cm^3 K mol^{-1} at 2 K. This magnetic variation as a function of temperature suggests the presence of ferromagnetic alignments among Mn(III) and Fe(III) spin centers.

We applied an analytical expression derived from a regular chain system ($H = -J\Sigma_i^{2n} S_i \cdot S_{i+1}$) to inspect the magnetic exchange coupling.[30]

$$\chi_m T = \frac{N\beta^2}{3k}\left[g^2\frac{1+u}{1-u} + \delta^2\frac{1-u}{1+u}\right] \quad (2)$$

The parameters are as follows: $g_{Mn}{}^e = g_{Mn}[S_{Mn}(S_{Mn}+1)]^{1/2}$, $g_{Fe}{}^e = g_{Fe}[S_{Fe}(S_{Fe}+1)]^{1/2}$, $J^e = J[S_{Mn}(S_{Mn}+1)S_{Fe}(S_{Fe}+1)]^{1/2}$, $g = (g_{Mn}{}^e + g_{Fe}{}^e)/2$, $\delta = (g_{Mn}{}^e - g_{Fe}{}^e)/2$, $u = \coth(J^e/kT) - (kT/J^e)$. A least-squares fitting gives roughly estimated parameters of $g_{Mn} = g_{Fe} = 2.13$ and $J = 1.79$ cm^{-1}.[31] We retained $g_{Mn} = g_{Fe}$ to accurately determine the two g parameters. This result discloses that spins in a chain are ferromagnetically coupled, which agrees well with **1**−**3** and most magnetic systems containing the *fac*-Fe tricyanide.[11,13] The saturation magnetization value in the $M(H)$ plot corresponds to 4.45 $N\beta$ at 7 T, which is analogous to the theoretical one calculated from the ferromagnetic result of two spin centers. The isofield curves in the reduced magnetization data at low temperatures (2−5 K) and high magnetic fields (1−7 T) are not superimposed (Supporting Information, Figure S2). To evaluate spin dynamics in **5**, ac magnetic data were collected at zero dc field, an ac amplitude of 5 G, and several oscillating frequencies, as given in Figure 11(b). The out-of-phase components (χ_m'') are frequency-dependent, pointing out a slow magnetic relaxation. Considering that there are no appreciable interchain contacts, this is reminiscent of a superparamagnetic-like behavior.[5,32]

Magnetostructural Correlation. To gain insight into the magnetic exchange mechanism we selected the dinuclear complex **3** for representative DFT calculations and were able to use the whole molecule in the calculations without artificial fragmentations.[33] The calculated exchange parameter based on Supporting Information, Table S1 is 6.4 cm^{-1}, which agrees well with the experimental parameter ($J = 4.91$ cm^{-1}).

The spin density distributions for the high-spin and low-spin states of **3** are illustrated in Figure 12. The spin density at the Fe center is fit for the occupation of a d_π orbital, while that at the Mn center is viewed as a distorted cube influenced from $t_{2g}{}^3$ and $e_g{}^1$ electronic configurations.[34] In terminal CN ligands it is obviously unveiled that the spin density of the N atom is mainly of π-type and has the same sign of the Fe spin density.

The magnetic natural orbitals[35] for the sextet state of **3** are depicted in Supporting Information, Figure S3. The magnetic orbitals of Mn are composed of a mixing of the $t_{2g}{}^3e_g{}^1$ set. The Fe center has the d_π orbital shape, which is identical to the spin density of the Fe ion. The magnetic

(30) Drillon, M.; Coronado, E.; Beltran, D.; Georges, R. *Chem. Phys.* **1983**, *79*, 449.
(31) Mn^{III} was assumed to act as a classical spin carrier with $S_{Mn} = 2$, leading to an effective alternating chain with $S_{Mn} = 2$ and $S_{Fe} = 1/2$. The magnetic model may be roughly applied to the system with the quantum spin $S_{Fe} = 1/2$.
(32) (a) Zheng, Y.-Z.; Lan, Y.; Wernsdorfer, W.; Anson, C. E.; Powell, A. K. *Chem.—Eur. J.* **2009**, *15*, 12566. (b) Yoo, H. S.; Ko, H. H.; Ryu, D. W.; Lee, J. W.; Yoon, J. H.; Lee, W. R.; Kim, H. C.; Koh, E. K.; Hong, C. S. *Inorg. Chem.* **2009**, *48*, 5617.
(33) Ruiz, E.; Cano, J.; Alvarez, S.; Alemany, P. *J. Comput. Chem.* **1999**, *20*, 1391.
(34) Euiz, E.; Rajaraman, G.; Alvarez, S.; Gillon, B.; Stride, J.; Clérac, R.; Larionova, J.; Decurtins, S. *Angew. Chem., Int. Ed.* **2005**, *44*, 271.
(35) Visinescu, D.; Desplanches, C.; Imaz, I.; Bahers, V.; Pradhan, R.; Villamena, F. A.; Guionneau, P.; Sutter, J.-P. *J. Am. Chem. Soc.* **2006**, *128*, 10202.

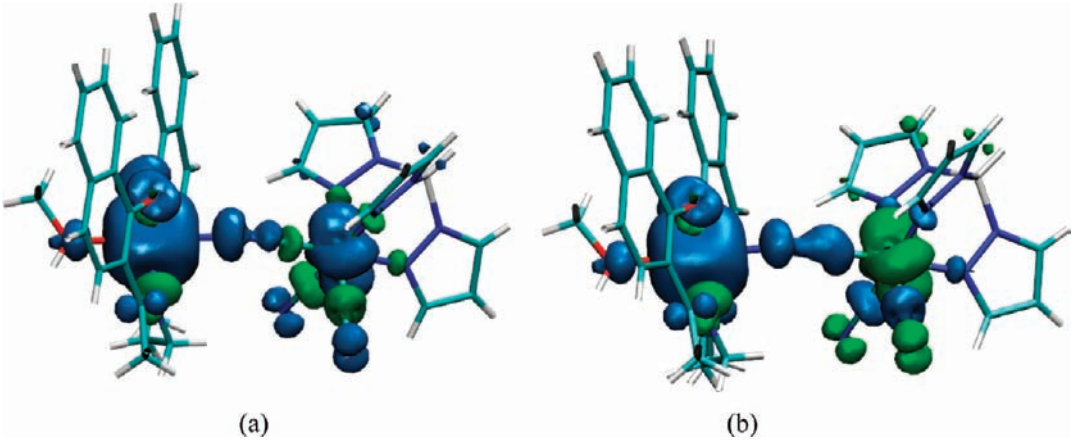

Figure 12. Spin density for the high-spin (sextet) state (a) and the broken-symmetry low-spin (quartet) state (b) of **3**. The excess α and β spins are shown in blue and green, respectively. The isovalue of the surface is 0.002 e Å^{-3}.

Table 3. Specific Structural Parameters[a] and Related Magnetic Coupling Constants for Fe(III)−Mn(III) Systems Constructed from *fac*-Fe^{III} Tricyanide

compounds	structure	Mn−N$_{cyano}$ (Å)	Mn−N≡C (deg)	J (cm^{-1})
1	dimer	2.334(2)	156.31(19)	7.48
2	dimer	2.307(4)	157.7(4)	6.66
3	dimer	2.247(3)	159.0(3)	4.91
4	dimer	2.298(4)	163.8(4)	−3.14
5	1D chain	2.372(3), 2.322(3)	149.3(3), 148.7(3)	1.79

[a] Mn−N$_{cyano}$ lengths and Mn−C≡N angles in the bridging pathways.

interaction between Fe(III) and Mn(III) can be understood by overall competition between antiferromagnetic (J_{AF}) and ferromagnetic (J_F) terms [$J = (1/n_A n_B)\Sigma_{ij} J_{ij} = J_{AF} + J_F$ where J_{ij} is the contribution of pairs of magnetic orbitals, n the number of unpaired electrons, and J_{AF} is proportional to the overlap integral (S) between the magnetic orbitals].[36] As seen in Supporting Information, Figure S3, two among five magnetic orbitals possess some mixing originated from each metal atom. This designates that S is not zero and the antiferromagnetic component (J_{AF}) exists.[35] However, in this case of **3**, the occupied Fe d orbital has a sufficiently small overlap with the magnetic orbitals on Mn, and hence the contribution from J_F prevails, finally leading to the observed ferromagnetic behavior in **3**. The similar orbital concept could be applied to complexes **1** and **2** exhibiting ferromagnetic interactions.

To get a more general magnetostructural relationship in the current Fe−C≡N−Mn platform, Mn−N$_{cyano}$ lengths, Mn−N≡C angles, and magnetic coupling constants of all samples are summarized in Table 3. The magnetic exchange couplings would be affected by the structural parameters relevant to the CN bridge between Mn(III) and Fe(III) centers. For the dimeric structures of **1**−**4**, the Mn−N$_{cyano}$ bond lengths tend to decline and the Mn−N≡C angles become more linear on moving from **1** to **4**. It is noticed that as the angle increases the magnitude of J is inclined to lessen gradually and eventually turns to be negative in **4**. This feature indicates that the increase of the Mn−N≡C angle toward linearity improves a degree of overlap of magnetic Fe and Mn d_π orbitals, resulting in

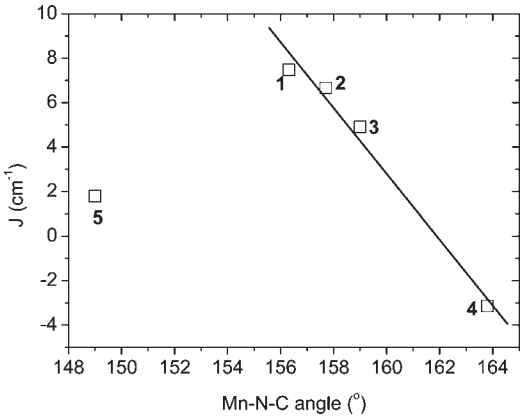

Figure 13. Correlation between magnetic coupling constants and Mn−N≡C angles of complexes **1**−**5**.

the dominance of J_{AF} over J_F at a critical angle and in turn favoring the antiferromagnetic couplings in **4**.[10] Similar magnetic features were also found in other cyanide-bridged Fe(III)−Mn(III) systems.[37,38] As far as the dimeric complexes are concerned, a linear relationship is established with an equation of J (cm^{-1}) = 239.63 − 1.48α where α is the Mn−N≡C angle (Figure 13). On the basis of the expression, the critical bond angle at which magnetic nature crosses is estimated to be 161.9°, which is in good agreement with the trend where magnetic interactions were mainly subject to change at a Mn−N≡C angle of 162°.[39] On the other hand, when the bending of the Mn−N≡C angle is much more severe as in **5**, the level of the orbital overlaps is likely pronounced because of relative rotations of pertinent magnetic orbitals, and then the J_{AF} term is reinforced to some extent.[40] Accordingly, the strength of the magnetic exchange coupling (J) diminishes as a consequence of competing effects from J_F and J_{AF}. This may be a

(36) Kahn, O..*Molecular Magnetism*; VCH: Weinheim, 1993.

(37) Ni, Z.-H.; Kou, H.-Z.; Zhang, L.-F.; Ge, C.; Cui, A.-L.; Wang, R.-J.; Li, Y.; Sato, O. *Angew. Chem., Int. Ed.* **2005**, *44*, 7742.

(38) Her, J.-H.; Stephens, P. W.; Kareis, C. M.; Moore, J. G.; Min, K. S.; Park, J. W.; Bali, G.; Kennon, B. S.; Miller, J. S. *Inorg. Chem.* **2010**, *49*, 1524.

(39) Ni, Z.-H.; Tao, J.; Wernsdorfer, W.; Cui, A.-L.; Kou, H.-Z. *Dalton Trans.* **2009**, 2788 and references therein.

(40) Zhang, Y.-Z.; Gao, S.; Wang, Z.-M.; Su, G.; Sun, H.-L.; Pan, F. *Inorg. Chem.* **2005**, *44*, 4534.

feasible scenario accounting for the lowered J value in **5** compared with those of **1**−**3**.

Conclusions

We have prepared and characterized four dimeric and one chain Fe(III)−Mn(III) compounds based on the $[(Tp)Fe(CN)_3]^-$ anionic precursor and the anisotropic Mn(III) Schiff base cations. Noncovalent contacts of hydrogen bonds, face-to-face $\pi-\pi$ contacts, and edge-to-face CH$-\pi$ forces exist among the dimeric molecules, which are responsible for enhancing molecular dimensions. On the contrary, no $\pi-\pi$ stacking interactions are detectable in the 1D chain compound. Magnetic data show that ferromagnetic couplings are present between Mn(III) and Fe(III) spin centers in **1**−**3** and **5**, while antiferromagnetic interactions are solely found in **4**. The magnetic couplings range from 1.79 to 7.48 cm^{-1} for the ferromagnetic systems and correspond to -1.40 cm^{-1} for the antiferromagnetic molecule. A slow magnetic relaxation is interestingly apparent in **5**, which emanates from the presence of well-isolated anisotropic chains. DFT calculations and structural analyses suggest that the observed magnetic behaviors are due mainly to the bending of the Mn−N≡C angle in the bridging pathway.

Acknowledgment. This work was supported by a National Research Foundation of Korea Grant funded by the Korean Government (No. 2009-0053164 and No. 2009-0071129). We thank Prof. Jeffrey R. Long for providing computational resources.

Supporting Information Available: X-ray crystallographic files in CIF format, additional synthetic, structural, magnetic, computational data for the complexes. This material is available free of charge via the Internet at http://pubs.acs.org.